Electronic structure of β-BaB_2O_4 and LiB_3O_5 nonlinear optical crystals

R. H. French
E. I. DuPont de Nemours and Company, Inc., Central Research and Development Department, E356/323 Experimental Station, Wilmington, Delaware 19880

J. W. Ling
Fujian Institute of Research on the Structure of Matter, Chinese Academy of Sciences, P. O. Box 143 Fuzhou, Fujian, China

F. S. Ohuchi
E. I. DuPont de Nemours and Company, Inc., Central Research and Development Department, E356/323 Experimental Station, Wilmington, Delaware

C. T. Chen
Fujian Institute of Research on the Structure of Matter, Chinese Academy of Sciences, P. O. Box 143 Fuzhou, Fujian, China
(Received 10 April 1991)

The relationship between the anionic groups of β-barium borate and lithium borate nonlinear optical (NLO) crystals and their bonding, electronic structure, and transmission cutoffs has been studied using the discrete variational self-consistent multipolar $X\alpha$ method [B. Delley and D. E. Ellis, J. Chem. Phys. **76**, 1949 (1982)] for the electronic structure of the borate anionic groups, coupled with experimental studies of the band gap, absorption edge, and valence bands, using vacuum ultraviolet spectroscopy and valence-band x-ray photoemission spectroscopy. The band gap of β-BaB_2O_4 (BBO) is 6.43 eV while LiB_3O_5(LBO) has a larger band gap of 7.78 eV. The structures of LBO and BBO differ principally in two aspects: the bonding in the borate anionic groups, and the isolation or linkage of the anionic groups in the crystal. BBO consists of $(B_3O_6)^{3-}$ anionic groups, with boron trigonally coordinated by oxygen; these groups are isolated in the crystal structure. LBO, however, is based on $(B_3O_7)^{5-}$ anionic groups, with boron either trigonally or tetrahedrally coordinated by oxygen, these groups are linked throughout the crystal. These structural differences between BBO and LBO lead to a larger band-gap energy in LBO. The linkage of LBO's anionic groups removes states from the top of the valence band which arise from the nonbonding terminal oxygen atoms present in BBO's unlinked anionic groups and also partially removes the π-conjugated orbitals associated with trigonally coordinated boron-oxygen bonding. The relationship between the crystal structure and the electronic structure can be seen as an extension of the molecular-engineering approach to search for additional NLO crystals in the uv range.

I. INTRODUCTION

The molecular engineering of nonlinear optical (NLO) and electro-optic materials has been a fruitful area of research since 1976.[1] Chen, in 1979, started using anionic group theory[2] and experimental methods to predict and grow many NLO crystals of the borate family. These have produced the ultraviolet (UV) NLO crystal β-BaB_2O_4 (BBO) (Ref. 3) along with other NLO crystals[4] such as LiB_3O_5 (LBO). These crystals have been developed as a direct result of molecular engineering in which localized molecular orbitals of the anionic groups such as $(B_3O_6)^{3-}$ and $(B_3O_7)^{5-}$, and the distortions of the idealized structures, have been analyzed to determine the microscopic contributions to the second-order susceptibility of the group. In order to engineer materials that can produce coherent radiation in the vacuum ultraviolet (VUV) region, it is necessary to understand the relationship between the electronic structure of the crystals and their spectroscopic properties.

The electronic structure of BBO has been calculated by Huang using the multiple-scattering-$X\alpha$ method,[5] while Zhang, Yang, and Zhang studied impurity-induced low-temperature absorption near the fundamental absorption edge of BBO.[6] Ching and co-workers have calculated the band structure and optical properties of LBO (Ref. 7) using the first-principles orthogonalized linear combination of atomic orbitals method.[8] Our present work focuses on understanding the electronic structures and VUV spectroscopic properties of BBO and LBO in terms of the basic structural units of these two crystals, i.e., the $(B_3O_6)^{3-}$ and $(B_3O_7)^{5-}$ anionic groups (Fig. 1). We have used the discrete variational self-consistent multipolar) $X\alpha$ (DV-SCM-$X\alpha$) method[9] to calculate the electronic structure of the anionic groups of BBO and LBO; and have also used VUV spectroscopy and valence-band x-ray photoemission spectroscopy (XPS) to investigate the band gap, band-to-band transitions and the valence-band density of states. On the basis of the calculations, we have determined the origin of the band-gap transitions in these materials and their relationship to the bonding of the anionic groups. This knowledge allows us to suggest

the type of bonding required to produce a borate crystal with a larger band gap and wider transparency region, potentially leading to additional VUV NLO crystals.

II. METHODS

A. Samples

The samples of BBO and LBO, from Fujian Institute, China, were large ($1\times1\times0.3$ cm^3) or larger crystals of good optical quality. There were some inclusions in the LBO crystal. The crystals were cut to appropriate size using a low-speed diamond saw and were optically polished on both sides using a ceria suspension as the polishing compound. The BBO crystal used for VUV spectroscopy was 0.13-cm thick, while the LBO crystal was 0.053-cm thick.

B. Vacuum ultraviolet spectroscopy

VUV transmittance and reflectance measurements were performed from 4.5 to 11 eV using a deuterium lamp source, in a vacuum of 10^{-8} Torr, with dispersive analysis of the light by a 1-m monochromator with a 600 groove/mm grating and a 1024 element detector.[10] This permitted a resolution of 0.3 nm. In regions of the spectrum where the crystals are transparent, the front-surface reflectance is augmented by light reflected from the back surface of the sample. Therefore, the measured reflectivity is greater than the single front-surface value. A Newton-Raphson method for two simultaneous equations[11] has been used to eliminate back-surface reflectance and calculate the absorption coefficient (α).[12] Band-gap energies were determined, assuming a direct band-gap model, by linear fitting to the steepest portion of a plot of α^2E^2 with the fitting performed over the range $15<\alpha<26$ cm^{-1} for both crystals, a range that corresponds to the fundamental absorption edge.

C. Valence-band x-ray photoemission spectroscopy

Valence-band x-ray photoemission spectra were obtained using monochromatic Al $K\alpha$ radiation. Small-spot optics (300 μm) and a charge-neutralization flood gun were used to avoid charging effects. The resolution of the measurements was 0.7 eV (Au $4f_{7/2}$ line width). The samples studied were small bars ($1.2\times1.2\times14$ mm^3) which were fractured *in situ* to avoid contamination.

D. Electronic structure calculations

The DV-SCM-$X\alpha$ method[9] has been used to calculate the electronic structures of the $(B_3O_6)^{3-}$ and $(B_3O_7)^{5-}$ clusters shown in Fig. 1, which are the basic anionic groups of the BBO and LBO crystals, respectively. The DV-SCM-$X\alpha$ method is appropriate since our main interest is in the $(B_3O_6)^{3-}$ or $(B_3O_7)^{5-}$ groups, and therefore a localized-molecular-orbital method for the electronic structure is reasonable; and also this method requires no shape approximation to the molecular potential or the charge density. This makes it convenient for treating covalent bonds in low-symmetry molecules such as these high-polarization anionic groups. Computationally, the DV-SCM-$X\alpha$ method is more efficient than the *ab initio* methods, especially when the number of basis functions is large. In this paper, we use numerical representations of atomlike functions as the variational basis funtions and select an $X\alpha$ parameter of 0.7.

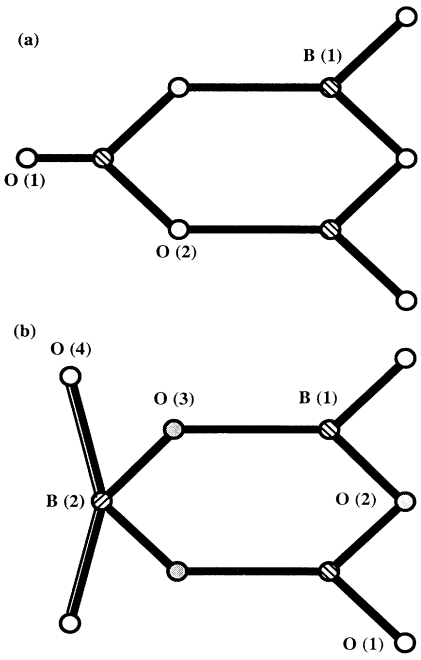

FIG. 1. The anionic groups of (a) $(B_3O_6)^{3-}$ for β-BaB_2O_4 (b) $(B_3O_7)^{5-}$ for LiB_3O_5.

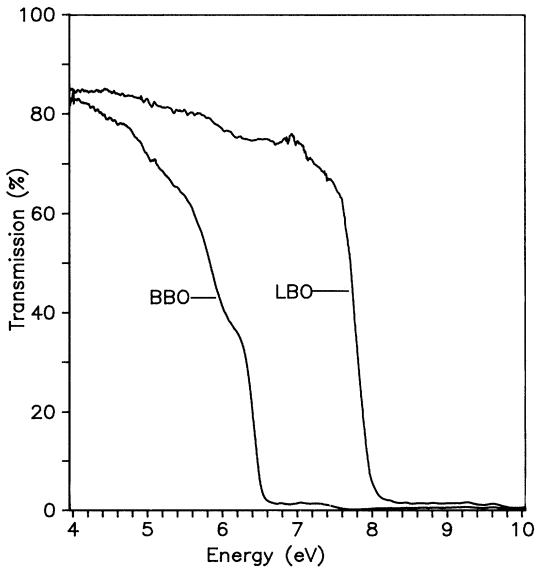

FIG. 2. Measured transmission cutoffs for BBO (0.13 cm thickness) at 193-nm and LBO (0.053 cm thickness) at 159 nm.

III. RESULTS

A. Vacuum ultraviolet spectroscopy

The transmittance limit of BBO and LBO differ substantially as shown in Fig. 2. BBO is transparent to 193 nm (6.43 eV), the limit of the air ultraviolet region, while LBO is transparent to 159 nm (7.78 eV) well into the vacuum ultraviolet region. In BBO we also observe the absorption-edge steps reported by Zhang, Yang, and Zhang.[6] The transparency of these borate NLO crystals into the VUV suggests the possibility of VUV second-harmonic generation in this family of materials. In Fig. 3, the absorption coefficients of the fundamental absorption edge are shown. The direct band-gap energies determined are 6.43 eV for BBO and 7.78 eV for LBO.

B. Valence-band XPS

The valence-band structures of BBO and LBO are shown in Figs. 4(a) and 5(a), respectively, and can be separated into an upper valence-band region derived from O 2*p* states and B-O bonding states and a lower valence-band region associated with O 2*s* states. Owing to charging of these insulating crystals, the binding energies shown are referenced to the valence-band maximum for each crystal (rather than to the absolute energy level of vacuum). The dominant features arise from transitions in the boron-oxygen anionic groups. The lower valence band highlights the structural differences between BBO and LBO. In BBO, both the O 1*s* and O 2*s* peaks split into doublets indicating two types of oxygen bonding, while in LBO they appear as singlets arising from a single type of oxygen bonding as shown in Fig. 6. In BBO the $(B_3O_6)^{3-}$ anionic groups are isolated, producing two oxygen environments; bridging oxygen atoms of the O(2) site and terminal oxygen atoms of the O(1) site which are only singly bonded to a boron. In LBO, the $(B_3O_7)^{5-}$ anionic group is not isolated in the crystal, but is linked throughout the crystal, such that each adjacent unit is rotated 90°, and all oxygen atoms in the $(B_3O_7)^{5-}$ are of a bridging nature.

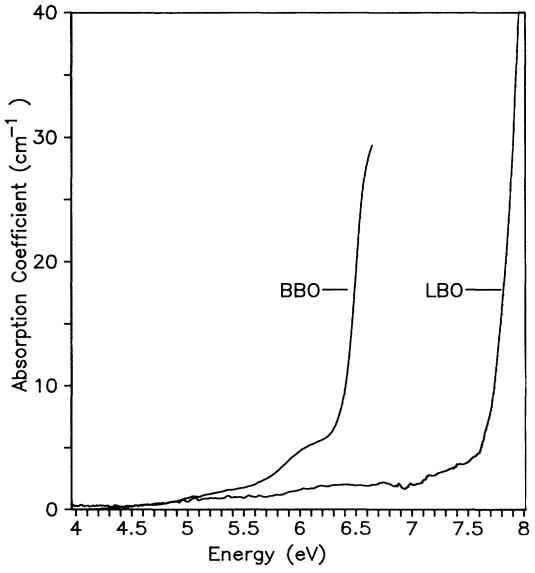

FIG. 3. Absorption coefficients of the fundamental absorption edge of BBO and LBO.

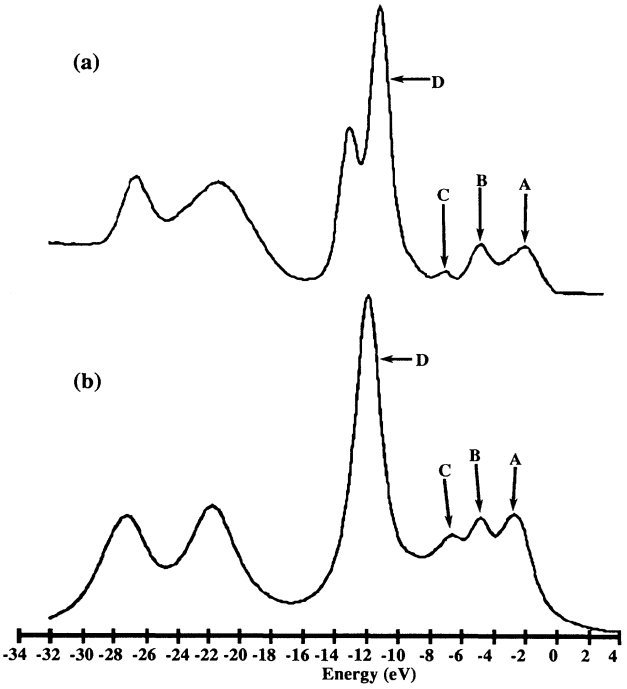

FIG. 4. (a) Valence-band XPS spectra for BBO showing the upper and lower valence-band regions and (b) calculated valence-band spectra with Lorentzian linewidth modification.

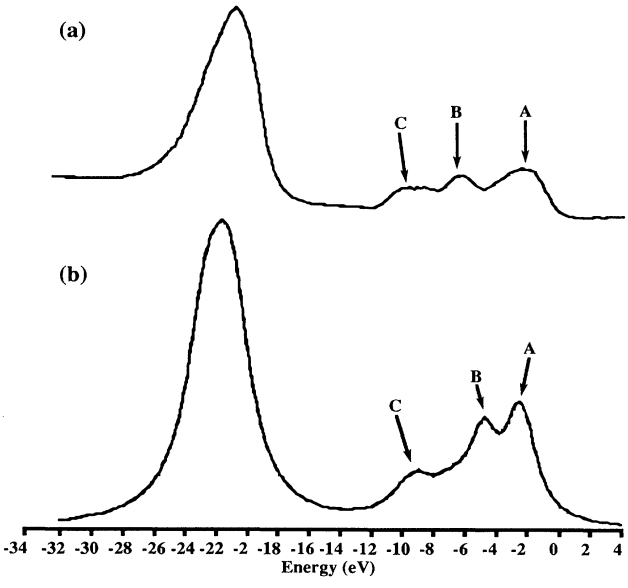

FIG. 5. (a) Valence-band XPS spectra for LBO showing the upper and lower valence-band regions and (b) calculated valence-band spectra with Lorentzian linewidth modification.

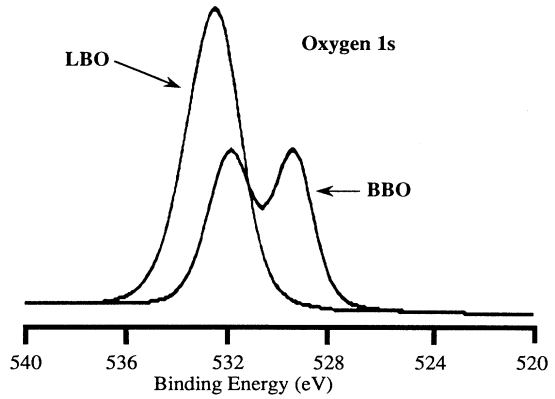

FIG. 6. Oxygen 1s core levels for BBO and LBO confirming the presence of two types of oxygen in BBO.

C. Electronic-structure calculations

1. β-BaB_2O_4 (BBO)

The BBO crystal is composed of the isolated $(B_3O_6)^{3-}$ anionic groups and Ba^{2+} cations. Raman spectroscopy indicates that the interaction between the $(B_3O_6)^{3-}$ anionic groups and Ba^{2+} cations is much weaker than the interaction between boron and oxygen atoms within the anionic groups.[13] The UV spectroscopy and valence-band XPS results indicate that the valence-band electronic structure of BBO is determined by the $(B_3O_6)^{3-}$ anionic groups. Hence, one can calculate the electronic structures of $(B_3O_6)^{3-}$ groups and Ba^{2+} cations separately. Assuming good agreement between the experimentally determined band-gap energy and the calculated valence-band to conduction-band transitions, one can conclude that the bottom of the conduction band also arises from the $(B_3O_6)^{3-}$ groups. This is supported by the calculated

TABLE I. The orbital energies of $(B_3O_6)^{3-}$, referenced to the valence-band maximum.

	Symmetry of orbitals	Orbital energy (eV) (referenced to valence-band maximum)	
	Conduction bands		
$9A_1'$	$\sigma^*, 2p_{x,y}, 2s$[O(2),O(1),B]	15.92	
Ba^{2+} 6s	Madelung-potential modified	14.3	
$11E'(2)$		14.25	
$10E'(2)$	$\sigma^*, 2p_{x,y}, 2s$[O(2),O(1),B]	12.01	
$8A_1'$		11.2	
$3A_2''$	π^*,[O(1),O(2),B]	8.02	
$3E''(2)$		6.2	
	Energy gap=6.2 eV		
	Valence bands		Peak
$2A_2'$	dangling bond, nonbonding O(1)	0	A
$9E'(2)$		−0.31	A
$2A_2''$	π,[O(1)]	−0.65	A
$2E''(2)$		−1.13	A
$8E'$	$\sigma, 2p_{x,y}$[O(2)]	−2.79	A
$7A_1'$	nonbonding, $2p_{x,y}$[O(1)]	−2.95	A
$7E'(2)$		−4.46	B
$1E''(2)$	π,[O(2)]	−4.89	B
$1A_2''$		−5.86	B
$6A_1'$	σ,[O(2)]	−7.07	C
$1A_2'$	$\sigma, 2p_{x,y}$[O(2),B]	−9.39	D
$6E'(2)$	$\sigma, 2p_{x,y}$[O(2)]	−9.6	D
Ba^{2+} 5p	Madelung-potential modified	−12	
$5A_1'$	$\sigma, 2s$[O(1)]	−19.66	
$5E'(2)$		−19.78	
$4E'(2)$	$\sigma, 2s$[O(2),B]	−25.04	
$4A_1'$		−26.25	

TABLE II. The energy levels of $(B_3O_7)^{5-}$ (eV), referenced to the valence-band maximum. Orbitals whose energies are in parentheses arise from the isolated nature of the $(B_3O_7)^{5-}$ cluster calculated and are not presented in the bulk crystal due to linkage of the $(B_3O_7)^{5-}$ anionic groups in the LBO crystal.

	Symmetry of orbitals	Orbital energy (eV) (referenced to valence-band maximum)	
	Conduction bands		
$12B_2$		20.5	
$16A_1$		18.4	
$11B_2$		17.74	
$15A_1$		17.04	
$8B_1$		15.33	
$14A_1$		15.17	
$10B_2$		15.12	
$13A_1$	$\sigma^*, 2s, 2p_{zy}$ (all O,B)	13.89	
$9B_2$		13.18	
$12A_1$	$\sigma^*, 2s, 2p_{yz}$[O(1),O(2),B(3),B(4)]	12.95	
$7B_1$	$\pi^*, 2p_x$[O(1),O(2),O(3),B(1),B(2)]	8.4	
$4A_2$		7.57	
	Energy gap=7.57 eV		
	Valence bands		Peak
$6B_1$		(2.54)	
$3A_2$		(2.11)	
$8B_2$	unlinked-cluster dangling bonds	(1.39)	
$11A_1$		(1.1)	
$7B_2$		(0.19)	
$5B_1$	$\pi, 2p_x$(O,B)	0	*A*
$10A_1$	unlinked-cluster dangling bond	(−0.11)	
$2A_2$	$\pi, 2p_x$(O,B)	−0.59	*A*
$4B_1$		−0.65	*A*
$9A_1$	σ[O(4)]	−1.48	*A*
$6B_2$	nonbonding $2p_y$[O(1),O(3)]	−1.63	*A*
$3B_1$	π[O(2),O(3)]	−2.59	*A*
$8A_1$	nonbonding $2p_{pz}$[O(3),O(2)]	−2.6	*A*
$7A_1$	nonbonding $2p_{yz}$[O(1)]	−2.74	*A*
$1A_2$	$\pi, 2p_x$[O(1),B(1),O(3)]	−2.75	*A*
$5B_2$	nonbonding $2p_{yz}$[O(2),O(3)]	−2.94	*A*
$2B_1$	$\pi, 2p_{yz}$[O(2),O(3)]	−4.28	*B*
$6A_1$	nonbonding [O(2),O(3)]	−5.02	*B*
$4B_2$	$\sigma, 2p_{yz}$[O(3),B(1)]	−6.79	*C*
$5A_1$	$\sigma, 2p_{yz}$[O(3)]	−7.27	*C*
$3B_2$	$\sigma, 2p_{yz}$[O(2),B(1)]	−7.73	*C*
$1B_1$	2*s*[O(9),O(10)]	(−13.32)	
$4A_1$	unlinked-cluster orbitals	(−14.35)	
$3A_1$	2*s*[O(1),O(2)]	(−16.03)	
$2B_2$	unlinked-cluster orbitals	(−16.16)	
$1B_2$	2*s*[O(3)]	−18.89	
$2A_1$	2*s*[O(2),O(3)]	−19.37	
$1A_1$		−20.69	

energy levels of isolated Ba^{2+} cation. The Ba 6s orbital is about 10 eV higher than the bottom of the BBO conduction band. The calculated energy levels of the isolated $(B_3O_6)^{3-}$ group and Ba^{2+} by the DV-SCM-$X\alpha$ approximation method are listed in Table I, and Fig. 4 shows their energy level structure with Lorentzian-linewidth modification.

In the upper valence band of BBO, a strong peak that arises from Ba 5p states is seen in the XPS, which is not evident in the electronic structure calculation of the $(B_3O_6)^{3-}$ anionic group. In the calculations, the isolated $(B_3O_6)^{3-}$ group, as illustrated in Fig. 1, has D_{3h} point-group symmetry and the polar axis is perpendicular to the plane of the (B_3O_6) group. If the energy levels of the Ba^{2+} are calculated as a free cation, the 5p orbital is situated at -46.0 eV, quite different from the Ba^{2+} 5p orbital energy seen experimentally near -12.0 eV (see Fig. 4). This difference arises because the Ba^{2+} cations and $(B_3O_6)^{3-}$ groups are both affected by the Madelung potential. As a result, the single-site-orbital[14] potential in the DV-SCM-$X\alpha$ method can be modified to include a Madelung potential acting on Ba^{2+}. This shifts the energy of 5p orbitals of Ba^{2+} from -46.0 to -12.0 eV. It is shown from the calculated result that the value of the Madelung potential U_M acting on Ba^{2+} is above 20.00 eV, in good agreement with the value directly calculated from the formula

$$U_M = -\frac{\alpha_M g_1 g_2}{R_0} . \quad (1)$$

Here R_0 is the nearest-neighbor separation between Ba^{2+} and the center of the $(B_3O_6)^{3-}$ group; $g_1 = +2$, the charge of Ba^{2+} cation and $g_2 = -3$, the charge of $(B_3O_6)^{3-}$; α_M is the Madelung constant.

From inspection of the eigenvectors for BBO, it is found that the orbitals $2A_2'$, $9E'(2)$, $8E'$, and $7A_1'$ in Table I are nonbonding orbitals of the O(1)-site terminal oxygen atom (see Fig. 1). The $2A_2''$ and $2E''(2)$ are π-conjugated orbitals mainly composed from O(1)-site atoms. These orbitals comprise peak A in the density of states of BBO shown in Fig. 4. $7E'(2)$, $1E''(2)$, and $1A_2''$ are the bonding π-conjugated orbitals composed of bridging oxygens of the O(2) site comprising peak B. The orbitals of σ type for O(2)-site atoms, a singlet $6A_1$, gives rise to peak C, whereas peak D, covered by the bands of Ba^{2+} 5p orbitals, and mainly related to the σ orbitals between O(2)- and B(1)-site atoms, are composed of a singlet $1A_2'$ and a doublet $6E'$.

The 5p orbitals of the Ba^{2+} cation are split into a singlet $5p_z$ along the z axis of the BBO lattice and a doublet $5P_{x,y}$ produced by the odd-ordered crystal-field potential, V_s.[15] This crystal field V_s reduces the energy of the $5P_z$ orbital and, therefore, the split 5p orbital with the lower density of states represents a $5p_z$ orbital while the $5p_{x,y}$ orbitals have a higher density of states.

2. LiB_3O_5 (LBO)

The basic anionic group of LBO is the $(B_3O_7)^{5-}$ anionic group. As in BBO, the interaction between the Li cation and the $(B_3O_7)^{5-}$ group is ignored. However, unlike BBO, the anionic groups in LBO are linked to each other. As a result, when the DV-SCM-$X\alpha$ method is used to calculate the energy levels of an isolated $(B_3O_7)^{5-}$ group, the existence of the nonbonding orbitals $6B_1$, $3A_2$, $8B_2$, $11A_1$, $7B_2$, and $10A_1$ of the isolated $(B_3O_7)^{5-}$ group, mainly related to O(1) and O(4) sites, should be similar to those of O(3) sites. We therefore have to map the above six orbitals to correspond to the O(3)-site orbitals. In the same way, $1B_1$, $4A_1$, $3A_1$, $2B_2$, mainly composed of 2s orbitals of O(1) and O(4) sites, should be similar to those of 2s orbitals of O(3) sites. The calculated results for linked $(B_3O_7)^{5-}$ groups are given in Table II, with the energy levels with Lorentzian linewidth modification shown in Fig. 5(a). The calculated results are compared in Fig. 5(b), and the agreement between them is quite satisfactory. Three energy bands appear, labeled A, B, and C, in the region from -13 to -2.0 eV in the spectrum. Band A is attributed to the energy levels $5B_1$, $2A_2$, $4B_1$, $6B_2$, $3B_1$, $8A_1$, $7A_1$, $1A_2$, $5B_2$, mainly composed of partly π-conjugated orbitals $2p_x$ of O and B atoms (see Fig. 1) and nonbonding $2p_{y,z}(0)$ orbitals. Band B is related to the singlet π-orbital $2B_1$ and another singlet nonbonding orbital $6A_1$ composed from O(2), O(3) sites and, finally, flat band C is related to the σ-type $2p_{y,z}$ orbitals of O(2), O(3) sites.

IV. DISCUSSION

The analysis of photoelectron spectra and our calculated results show that the optical absorption edge in the UV region of BBO and LBO crystals is mainly determined by the transitions from valence band A to the conduction bands. In BBO band A arises from the nonbonding orbitals and π-conjugated orbitals of the $(B_3O_6)^{3-}$ anionic group. The calculated band gap between band A and the conduction bands is about 6.2 eV compared with the measured direct band-gap energy of 6.43 eV for the BBO crystal. Moreover, the 5p orbitals of the barium ion are close to band D of the $(B_3O_6)^{3-}$ group, arising from σ-type orbitals. Thus, if one desires a borate with a shorter-wavelength, or higher-energy, absorption edge than BBO, the best way is to remove the nonbonding orbitals and destroy the π-conjugated orbitals that comprise the top of the valence band of the $(B_3O_6)^{3-}$ group. LBO is a good example of this strategy. The continuous network of $(B_3O_7)^{5-}$ groups with interstitial lithium cations form an endless spiral running parallel to one axis. As a result, all the nonbonding orbitals on BBO are removed in LBO. At the same time the π-conjugated orbitals of BBO are partially removed in LBO as one boron atom of the $(B_3O_7)^{5-}$ group changes from trigonal to tetrahedral coordination. This results in a wider calculated band gap for linked $(B_3O_7)^{5-}$ anionic groups of about 7.57 eV, compared with the measured LBO band-gap energy of 7.78 eV. The band structure of LBO calculated by Xu and Ching[7] gives a band-gap energy of 7.37 eV, which underestimates the experimental value of the gap as expected for a local-density-approximation calculation. Xu and Ching also confirm that the band gap and elec-

tronic structure of LBO are dominated by the localized trigonal and tetrahedral boron-oxygen groups, further supporting our localized method for this problem.

The π-conjugated orbitals existing in the $(B_3O_6)^{3-}$ group are only partly destroyed in the $(B_3O_7)^{5-}$ group. We believe that if all the π-conjugated orbitals of the $(B_3O_7)^{5-}$ group can be destroyed by changing all the boron atoms in the $(B_3O_6)^{3-}$ group from trigonal to tetrahedral coordination, forming a fully tetrahedrally bonded boron-oxygen compound, a shorter-wavelength or higher-energy optical absorption edge in the VUV region can be achieved. We hope that this assertion will be proven as soon as possible.

V. CONCLUSIONS

The relationship between the anionic groups of β barium and lithium borate nonlinear optical crystals and their bonding, electronic structure, and transmission cutoffs has been studied using the DV-SCM-$X\alpha$ method for calculating the electronic structure of the borate anionic groups. The results have been confirmed by experimental investigations of the band gap, absorption edge, and valence bands, using vacuum ultraviolet (VUV) spectroscopy and valence-band x-ray photoemission spectroscopy (XPS). The direct band-gap energy of β-BaB_2O_4 is 6.43 eV while LiB_3O_5 has a larger direct band-gap energy of 7.78 eV. The larger band gap and transparency region of LiB_3O_5 arise from two causes, the linkage of the anionic groups in the crystal and reduced π-conjugated bonding in the borate anionic groups. β-BaB_2O_4 contains isolated $(B_3O_6)^{3-}$ anionic groups in the crystal structure with trigonally coordinated boron-oxygen bonding in the groups, whereas LiB_3O_5 consists of $(B_3O_7)^{5-}$ anionic groups which are linked throughout the crystal and contain both trigonally and tetrahedrally coordinated boron-oxygen bonding. These structural differences result in the removal of states from the top of the valence band which arise from the nonbonding terminal oxygen bonds of the unlinked groups of BBO and also partially removes the π-conjugated bonds associated with trigonally coordinated boron-oxygen bonding in the anionic groups, thereby increasing the band-gap energy. This detailed understanding of the relationship between the atomic and electronic structure of these materials provides a powerful tool for the molecular engineering of additional NLO cyrstals in the UV range.

ACKNOWLEDGMENTS

This work was partially supported by the Science Fund Grant No. 1860283 of the Chinese Academy of Sciences. Two of the authors, C.T.C. and J.W.L., are very grateful to Wu Kechen for his assistance with the electronic structural calculations of the LBO crystal. We would like to acknowledge the assistance of D. J. Jones in the VUV spectroscopy, and S. Loughin for a critical reading of the manuscript.

[1]C. T. Chen and G. Liu, Ann. Rev. Mater. Sci. **16**, 203 (1986).

[2]C. T. Chen, Rev. Chin. Sci. B (to be published); C. T. Chen and S. X. Chen, Acta Phys. Sin. **29**, 1000 (1980).

[3]C. T. Chen, B. C. Wu, A. D. Jiang, and G. M. You, Sci. Sinica Series b **13**, 235 (1985); J. Liebertz and S. Stahr, Z. Kristallogr. **165**, 91 (1983); R. Frohlich, *ibid.* **168**, 109 (1984); S. Lu, M. Ho, and J. Huang, Acta Phys. Sin. **31**, 948 (1982).

[4]Chuangtian Chen, Yicheng Wu, Aidong, Jiang, Bochang Wu, Guiming You, Rukang Li, and Shujie Lin, J. Opt. Soc. Am. B **6**, 616 (1989); C. T. Chen, Y. Wu, and R. Li, Int. Rev. Phys. Chem. (to be published); H. Konig and A. Hoppe, Z. Anorg. Allg. Chem. **439**, 71 (1979); M. Lhara, M. Yuge, and J. Krogh-Meo, Yogyo Kyokaishi **88**, 179 (1980).

[5]J. Huang and D. Wang, Chin. Phys. Lett. **3**, 157 (1986).

[6]G. Zhang, Y. Yang, and C. Zhang, Appl. Phys. Lett. **53**, 1019 (1988).

[7]Y. N. Xu and W. Y. Ching, Phys. Rev. B **41**, 5471 (1990).

[8]W. Y. Ching, J. Am. Ceram. Soc. **73**, 3135 (1991).

[9]B. Delley and D. E. Ellis, J. Chem. Phys. **76**, 1949 (1982).

[10]R. H. French, Phys. Scr. **41**, 404 (1990); M. L. Bortz and R. H. French, Appl. Phys. Lett. **55**, 1955 (1989); M. L. Bortz, R. H. French, D. J. Jones, R. V. Kasowski, and F. S. Ohuchi, Phys. Scr. **41**, 537 (1990); R. H. French, J. Am. Ceram. Soc. **73**, 477 (1990).

[11]See, for example, W. H. Press, B. P. Flannery, S. A. Teukolsky, and W. T. Vetterling, *Numerical Recipes—The Art of Scientific Computing* (Cambridge University Press, Cambridge, England, 1986), p. 269.

[12]M. E. Innocenzi, R. T. Swimm, M. Bass, R. H. French, A. B. Villaverde, and M. R. Kokta, J. Appl. Phys. **67**, 7542 (1990); M. E. Innocenzi, R. T. Swimm, M. Bass, R. H. French, and M. R. Kokta, *ibid.* **68**, 1200 (1990).

[13]G. Zhang, Y. Yang, and B. Wu, Acta Opt. Sin. **5**, 548 (1985).

[14]F. W. Averill and D. E. Ellis, J. Chem. Phys. **59**, 6412 (1973).

[15]R. K. Li and C. T. Chen, Acta Phys. Sin. **34**, 823 (1986).